


A cohesive approach at estimating water saturation in a low-resistivity pay carbonate reservoir and its validation

Adedapo Awolayo¹  · Ayham Ashqar² · Miho Uchida² · Andi Ahmad Salahuddin² · Saheed Olawale Olayiwola²

Received: 17 November 2015 / Accepted: 5 January 2017 / Published online: 3 February 2017
© The Author(s) 2017. This article is published with open access at Springerlink.com

Abstract Carbonate reservoir characterization and fluid quantification seem more challenging than those of sandstone reservoirs. The intricacy in the estimation of accurate hydrocarbon saturation is owed to their complex and heterogeneous pore structures, and mineralogy. Traditionally, resistivity-based logs are used to identify pay intervals based on the resistivity contrast between reservoir fluids. However, few pay intervals show reservoir fluids of similar resistivity which weaken reliance on the hydrocarbon saturation quantified from logs taken from such intervals. The potential of such intervals is sometimes neglected. In this case, the studied reservoir showed low resistivity. High water saturation was estimated, while downhole fluid analysis identified mobile oil, and the formation produced dry or nearly dry oil. Because of the complexity of Low-resistivity pay (LRP) reservoirs, its cause should be determined a priori to applying a solution. Several reasons were identified to be responsible for this phenomenon from the integration of thin section, nuclear magnetic resonance (NMR) and mercury injection capillary pressure (MICP) data—among which were the presence of microporosity, fractures, paramagnetic minerals, and deep conductive borehole mud invasion. In this paper, we integrated various information coming from geology (e.g., thin section, X-ray diffraction (XRD)), formation pressure and well production tests, NMR, MICP, and Dean–Stark data. We discussed the

observed variations in quantifying water saturation in LRP interval and their related discrepancies. The nonresistivity-based methods, used in this study, are Sigma log, capillary pressure-based (MICP, centrifuge, and porous plate), and Dean–Stark measurements. The successful integration of these saturation estimation methods captured the uncertainty and improved our understanding of the reservoir properties. This enhanced our capability to develop a robust and reliable saturation model. This model was validated with data acquired from a newly drilled appraisal well, which affirmed a deeper free water level as compared to the previous prognosis, hence an oil pool extension. Further analysis confirmed that the major causes of LRP in the studied reservoir were the presence of microporosity and high saline mud invasion. The integration of data from these various sources added confidence to the estimation of water saturation in the studied reservoir and thus improved reserves estimation and generated reservoir simulation for accurate history matching, production forecasting, and optimized field development plan.

Keywords Water saturation · Carbonate reservoirs · Low-resistivity pay · Core analysis · Field development

List of symbols

\sum_H	Sigma of the hydrocarbon
\sum_{LOG}	Sigma of the formation
\sum_M	Sigma of the matrix
\sum_W	Sigma of the water
k	Permeability
ϕ	Porosity
P_C	Capillary pressure
S_W	Water saturation
θ	Contact angle
σ	Interfacial tension

✉ Adedapo Awolayo
adedapo.awolayo@ucalgary.ca

¹ Department of Chemical and Petroleum Engineering, Schulich School of Engineering, University of Calgary, 2500 University Drive NW, Calgary, AB T2N 1N4, Canada

² Abu Dhabi Company for Onshore Petroleum Operations Ltd. (ADCO), P.O.Box 270, Abu Dhabi, UAE

J	Leverett J -function
m	Cementation exponent
n	Saturation exponent
R_w	Formation water resistivity
R_t	True formation measured resistivity

Abbreviations

BF	Bacinella floatstone
DST	Drill stem test
FWL	Free water level
HRSS	High resolution sequence stratigraphic
HST	Highstand system tracks
LRP	Low-resistivity pay
LWD	Logging while drilling
MICP	Mercury injection capillary pressure
NMR	Nuclear magnetic resonance
OBG	Ooid bacinella grainstone
OH	Open-hole
OWC	Oil water contact
PBP	Peloidal burrowed packstone
PG	Petrophysical groups
PNC	Pulsed neutron capture
PSD	Pore size distribution
PTR	Pore throat radius
SB	Sequence boundary
SCAL	Special core analysis
STOIP	Stock tank oil in place
TST	Transgressive system tract
UV	Ultraviolet
WBM	Water base mud
WFT	Wireline formation tester
XRD	Xray diffraction

Introduction

LRP reservoir was first discovered in a sandstone reservoir within the Gulf of Mexico (Boyd et al. 1995) and has progressively been at the frontline of several industrial projects that involves deep water exploration and brown-field development. It has been described as hydrocarbon-bearing zone that appears as water interval based on open-hole resistivity measurements. Meanwhile, such intervals show strong hydrocarbon on mud logs and produce hydrocarbon as either gas or oil with little or no water cut from core studies, pressure and production tests (Pittman 1971; Keith and Pittman 1983; Worthington 2000). Additionally, the LRP intervals are commonly identified with high water saturation, which makes such intervals of low interest to the extent that they are discarded as attractive to appraise, particularly when oil prices are low. Typically, LRP zones are characterized by formation interval, with moderate to high porosities, showing extremely low

resistivity that are often less than 3 Ω -m and most frequently encountered in areas with saline formation water (Griffiths et al. 2006; Obeidi et al. 2010; Worthington 2000; Farouk et al. 2014; Uchida et al. 2015). While Boyd et al. (1995) proposed that the resistivity range is between 0.5 and 5 Ω -m, several other researchers, like Zhao et al. (2000), stated that LRP can be identified by the ratio of the pay zone to the water-bearing zone and this ratio is considered to be in the range of 2.

LRP occurs in both clastics and carbonates, while in carbonates, it has been reported to be as a result of either or a combination of deep high saline mud invasion, presence of conductive minerals, presence of microporosity, and anisotropic effect due to drilling high angle wells within thin reservoirs (Griffiths et al. 2006; Obeidi et al. 2010; Chu and Steckhan 2011). Most especially, tight carbonates are often affected by the deep invasion of conductive mud filtrate, which consecutively affects deep resistivity reading (Souvick 2003). It is imperative to determine the main causes of LRP so as to capture the uncertainty range and define the best technique to evaluate the reservoir parameters. Despite the vast amount of research done in the past two decades to address this phenomenon, this issue still persists and no unique technique has been established, particularly in carbonate reservoirs to the best of our knowledge. The disparity between the resistivity-derived saturation and other various sources demands a reservoir-specific in-depth study to identify the main cause of such disagreement. Several causes of LRP reported and the corresponding solution proposed are discussed below:

- **High saline muds deep invasion:** Most often deep invasion occurs, which remarkably influence deep resistivity logs when drilling wells with high saline muds. Consequently, the influence of mud invasion becomes too difficult to ascertain such that high water saturation is estimated from the low-resistivity reading (Souvick 2003). One of the techniques proposed to tackle deep invasion problem is running resistivity logging-while-drilling (LWD) since LWD time is less compared to its wireline equivalent (Boyd et al. 1995). Obeidi et al. (2010) proposed to use pulsed neutron capture (PNC) to evaluate LRP reservoirs. This technique uses chlorine to control the rate of capture of the thermal neutron in the formation. However, the proposed suggestion may not be suitable as the technique is hampered by shallow depth of investigation. Similarly, LRP intervals are created by open fractures (either induced or natural) where high saline muds from the wellbore can easily penetrate through the fractures (Asquith 1985). Borehole imaging tools are capable of revealing these fractures. An integration of these tools with resistivity logs could improve the

estimation of the hydrocarbon saturation (Souvick 2003; Petricola et al. 2002).

- **Microporosity:** The presence of bimodal pore systems in carbonates is considered a common factor responsible for LRP intervals (Pittman 1971). In this regard, the high capillary bound water is mainly associated with rock grain size. The smaller the grain size, the higher the surface to volume ratio, and the greater the tendency for grains to hold a significant volume of water. Typically, in carbonate reservoirs, the macropores hold and produce the moveable hydrocarbons due to their lower entry pressure, which is adjacent to micropores holding the immobile highly saline formation water due to the high entry pressure. Such micropores can be present in different forms as highlighted by Uchida et al. (2015) and Salahuddin et al. (2015). Hassan and Kerans (2013) investigated the geological consequences of LRP in carbonate reservoirs and reported that the microporosity is 70% of the total porosity in all facies studied from 14 core plugs. They concluded that these microporous zones contained capillary bound formation brine which provided a continuous path for electric current. Hence, the available hydrocarbon was masked and this caused a significant underestimation of the true oil saturation. One of the proffered solutions is to use core-measured cementation exponent (m) and saturation exponent (n) if no deep invasion was encountered. Also, the use of NMR, which differentiates bound water from free water, was suggested.
- **Presence of paramagnetic minerals:** Paramagnetic minerals such as pyrite have the capability to reduce the log resistivity reading. Their effects vary with their morphology and distribution. The solution that has been proffered involved computation of the mineral volume before assigning the mineral conductivity to finally estimate the accurate hydrocarbon saturation (Souvick 2003). Lithology identification log has commonly been used to estimate the volume of different minerals, while XRD has been used to compute the minerals relative fractions.
- **Laminated formations:** Another common cause is laminated formations, and a typical example is a thin-bedded formation with variations of fine-grained and coarse-grained carbonates. Fine-grained (like mud-dominated packstone) are often saturated with formation water due to their high entry capillary pressure, while coarse-grained (e.g., grain-dominated packstone) are usually filled with hydrocarbon due to the associated low entry capillary pressure. The resistivity response of the hydrocarbon layer is often averaged with the surrounding muddy layers by the resistivity tool, leading to low resistivity and consequently high water saturation. This

occurs when the bed thickness is equal or less than the vertical resolution of the resistivity tool (Hassan and Kerans 2013). Gyllensten et al. (2007) suggested that the impact of the laminated shale on a sandstone reservoir are same as that of micritized grains in a carbonate reservoir. The authors proposed the use of a resistivity tool that is perpendicular to the bedding to evaluate such reservoir. However, this is not always the case, microporous pore space is known to distribute in other shapes such as dispersed, using vertical resistivity will not detect dispersed micrities.

Meanwhile, carbonate reservoirs hold a larger percentage of the world's proven reserves (Awolayo et al. 2015); their characterization will continue to remain enormously difficult due to LRP among other concerns. With this background knowledge in mind, this paper proposes a novel workflow to evaluate LRP reservoirs and develop a robust model to unveil the reservoir potential. The developed workflow is aimed to be the best practice to define hydrocarbon saturation through an interdisciplinary study by integrating conventional logs, core analysis (porosity, permeability, Dean–Stark, MICP, porous plate, and centrifuge capillary pressures), wireline formation tester (WFT), and drill stem test (DST) results. Lastly, we present the validation of the new model with data acquired from a new well drilled to the newly identified free water level (FWL).

Geological interpretation

The studied field is located onshore Abu Dhabi and formed as a faulted low-relief four-way anticline closure and oil bearing, separated by a major NW–SE trending fault into two areas, namely Area A and Area B (Fig. 1). The studied reservoir is a part of Lekhwair Formations that belongs to Thamama Group. It was deposited in carbonate platform environment during Barremian age which is equivalent to Lower Cretaceous system (see Fig. 2). The reservoir is 55 ft thick, highly heterogeneous with moderate to good porosity as high as 23%, while the permeability ranges from 0.02 mD to more than 1 D (Salahuddin et al. 2015). The low pay reservoir was noted in late 1990 when a well produced oil with zero percent water cut, though log interpretation indicated high water saturation, formation pressures taken across the reservoir showed an oil gradient and mud logs showed strong presence of hydrocarbon.

Sequence stratigraphic framework

The Lekhwair Formation corresponds to the early-mid transgressive system tract (TST) of a second-order

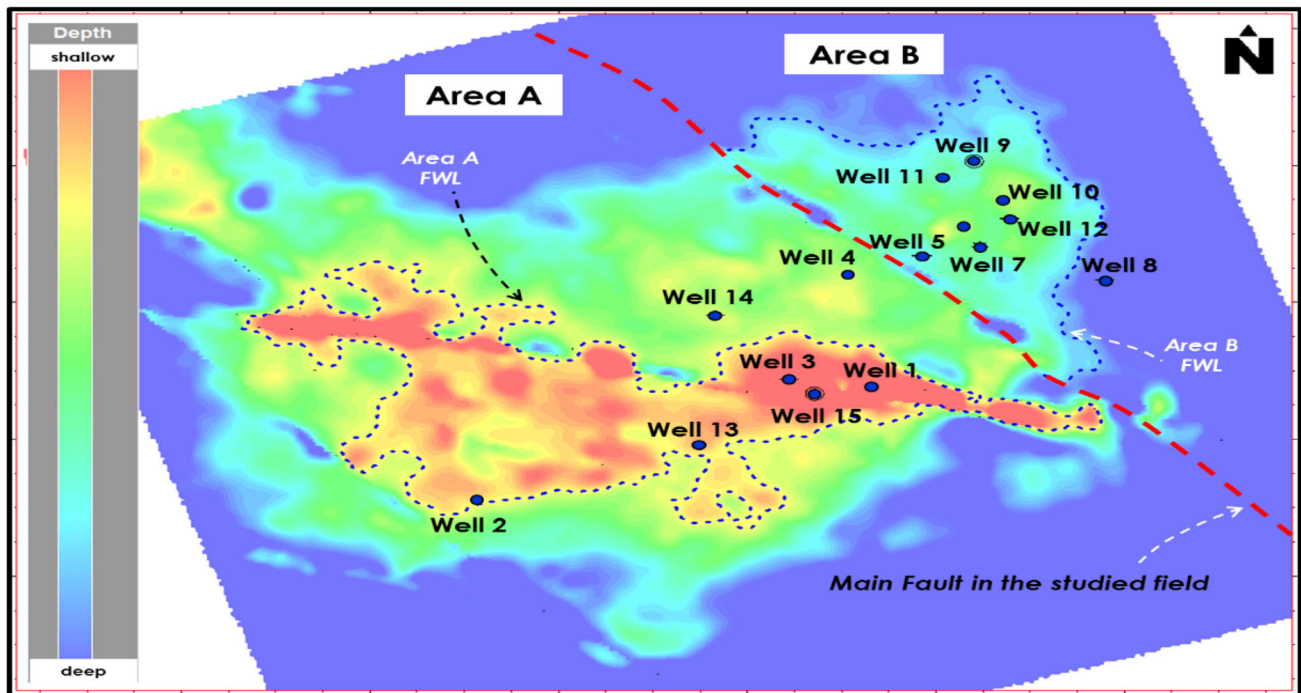


Fig. 1 Reservoir Top depth map and key wells location

supersequence. The formation is built by two-third-order composite sequences (Fig. 2). The studied reservoir corresponds to the latest highstand system tract (HST) of third-order composite sequence (Strohmenger et al. 2006). The three-fourth-order parasequence sets that built this upper third-order composite sequences show a combination of retrogradational and progradational stacking patterns (Rebelle and Al Nuaimi 2006). Detailed core description in Fig. 3 signified the presence of three HST separated by two TST. The reservoir shows relatively less diverse fossils characterized by a combination of high-energy oolitic grainstone and low-energy peloidal packstone and Bacinella floatstone.

Facies and depositional environment

The sedimentological analysis was performed over 300 ft of core from 10 wells providing excellent areal and vertical datasets covering the studied area. In addition, more than 100 of thin sections were described to assess faunal contents and rock textures. The thin sections were impregnated with blue dyed epoxy and stained with alizarin red S. Further integration with routine core analysis and MICP gave fundamental information on the composition and microtexture of the facies. This also contributed toward understanding the diagenetic overprint and pore systems characteristics of the studied reservoir. Three (3) lithofacies types were defined for the studied reservoir of Lekhwair Formation

(Fig. 4) based on the modified Dunham's classification (Dunham 1962), namely:

1. PBP (peloidal burrowed packstone): brownish packstone with abundant peloids and associated small bivalves, foraminiferas and echinoids. Bioturbation is quite common.
2. BF (Bacinella floatstone): floatstone with centimetric Bacinella, associated with entire bivalves, rudists and echinoids. Bivalves abundance confirming a low-energy deposit.
3. OBG (oid Bacinella grainstone): light brown grainstone with ooids, large Bacinella, peloids, foraminiferas, bivalves and echinoids. Matrix between the Bacinellas is composed of a peloidal grainstone to packstone, locally cemented by syntaxial cement around echinoids fragments. The interpreted depositional environment ranged from inner lagoon to inner shoal as simply illustrated in Fig. 4.

Depositional and diagenetic controls on LRP presence

Previous studies showed that complex pore distributions in carbonates play a key role in determining accurate hydrocarbon saturations. Pittman (1971) and Keith and Pittman (1983) discovered that the presence of bimodal pore systems in carbonates commonly contributes to LRP interval phenomena. The distribution of bimodal pores includes

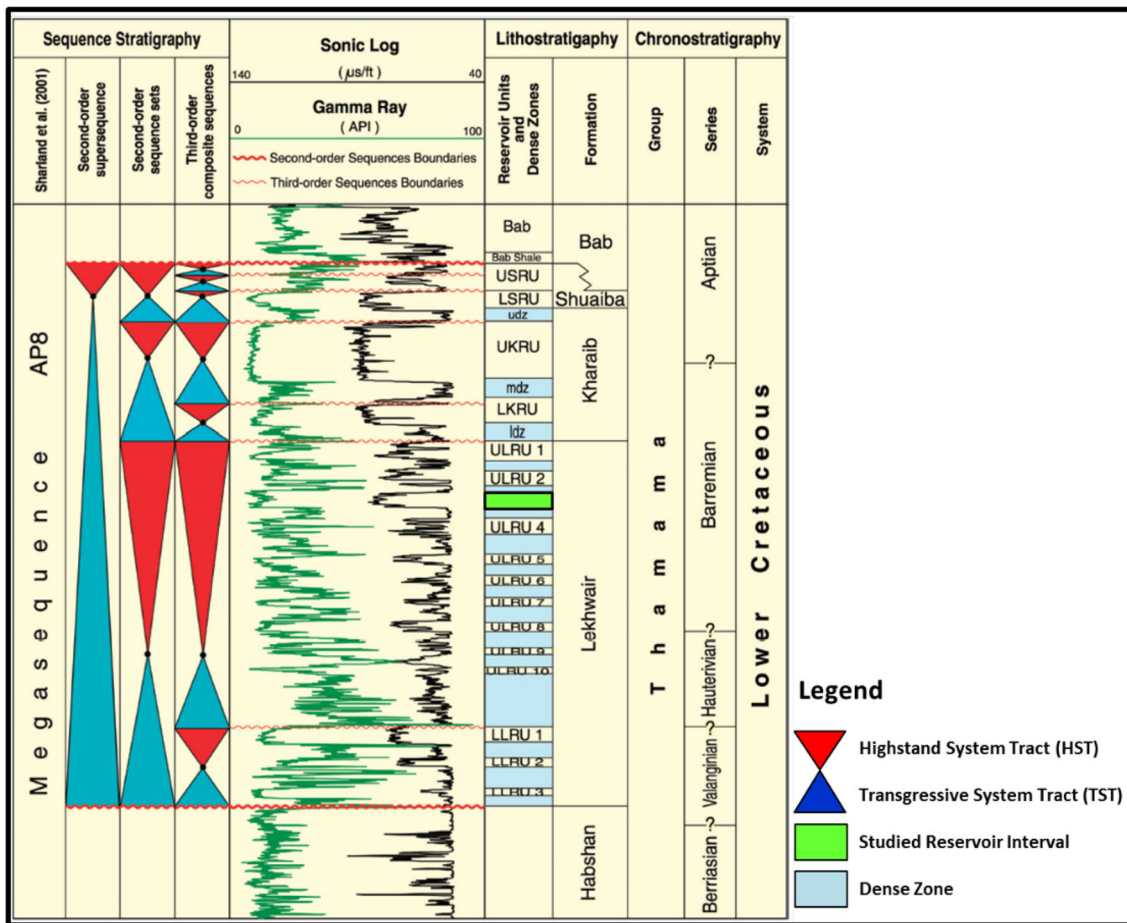


Fig. 2 Upper Thamama Group (Lower Cretaceous) sequence stratigraphic framework (Strohmenger et al. 2004, 2006)

intergranular macropores and adjacent micropores. These micropores can be present between the micritic materials in lime mud as well as between the micritic materials filling the grains. As mentioned earlier, this can create a short circuit of the measured current resulting in low-resistivity reading and consequently yielding a significant underestimation of the true water saturation.

The diagenesis process that took place on this studied reservoir was explained through core description and thin sections observations. The identified diagenetic process that took place includes micritization, cementation, replacement (pinitization), and burial compaction. Micritization involved the formation of micrite envelope around the grains, where the porosity and permeability are reduced, by filling the original pore space of the rock. Cementation took place with different intensities and types. Several types of cement have been observed, which are calcite fringe rim, epitaxial cement, and sparry calcite. They developed around the grains, which is an indication of early diagenesis (Fig. 5). Compaction due to overburden pressure resulted in further reduction in rock properties and thickness.

Thin section analysis further revealed that the presence of micrites and micritized grains was the main factor responsible for the LRP interval. In other words, micropores responsible for the LRP existence had a strong relationship with the abundance of micrites and micritized grains as shown in Fig. 6. Therefore, it was important to understand the geological condition that control the spatial distribution of micrites and/or micritization and their associated facies within the sequence stratigraphic framework to better evaluate the LRP intervals for future modeling purposes.

Distribution of micropores

Micrites are composed of microcrystalline calcite with 1–4 μm diameter crystals (Folk 1959). Micrite as a component of carbonate rocks can be present as a matrix or as micrite envelopes around allochems. Micrite is generated by chemical precipitation, from disaggregation of peloids, or by micritization.

Micritization is a process by which grains in a carbonate sediment (allochems) are transformed into fine-grained calcite from their original form usually removing their internal

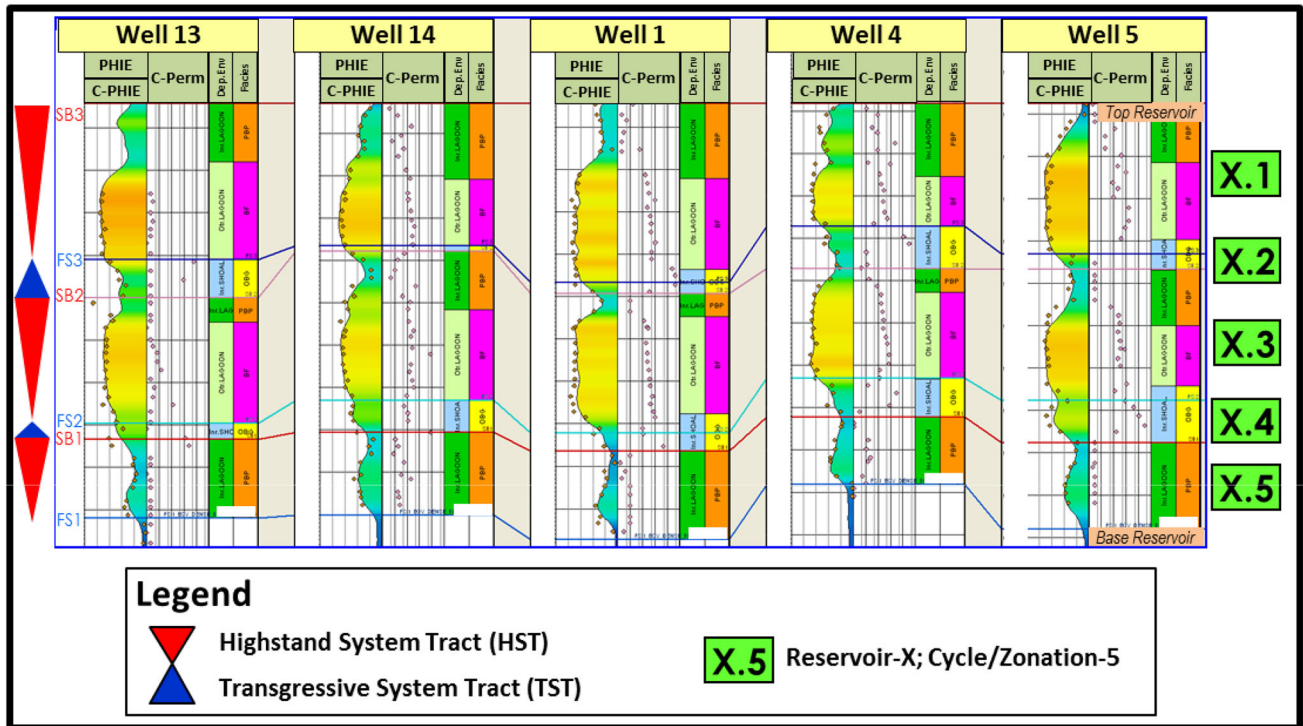


Fig. 3 Well cross section on some key cored wells of the studied field showing the established high-resolution sequence stratigraphic (HRSS) framework and the vertical and horizontal distribution of facies

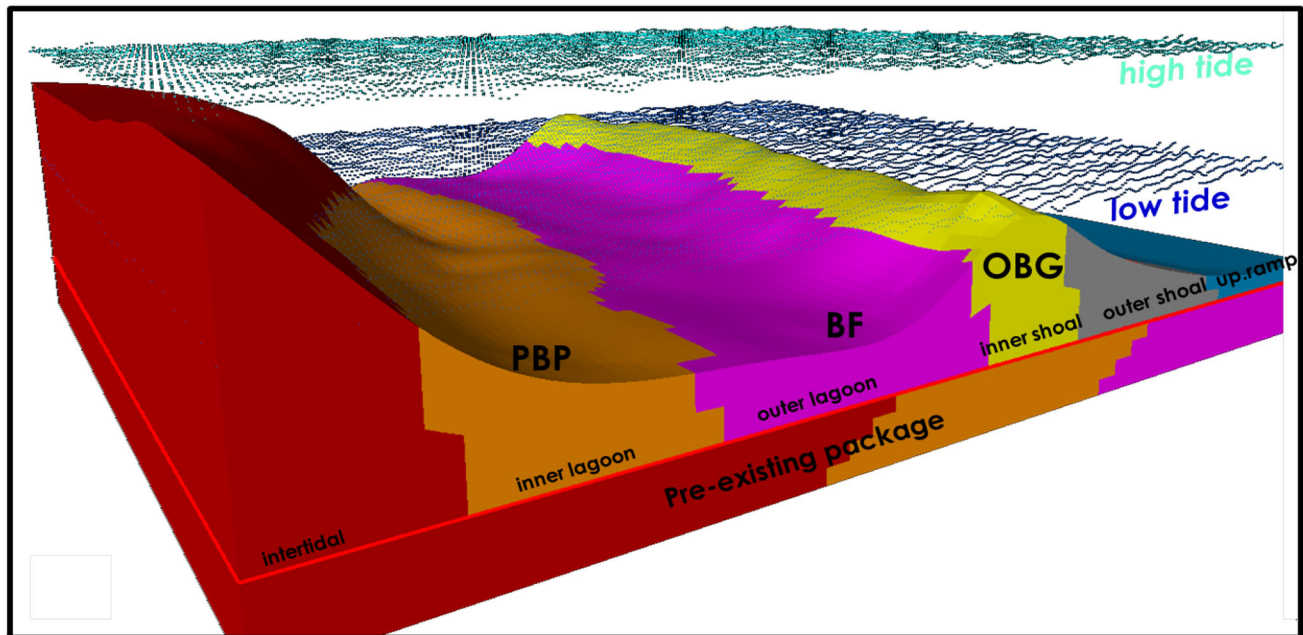


Fig. 4 Paleo-bathymetric profile showing the interpreted depositional environment and lateral facies distribution. *PBP* peloidal burrowed packstone; *BF* Bacinella floatstone; *OBG* ooid Bacinella grainstone

structure. Micritization occurs due to the action of endolithic algae (nonskeletal blue green algae) which bore into bioclasts. The early stages of micritization lead to the formation of micrite envelope, often with an irregular internal surface.

More intense micritization, however, can lead to the complete replacement of bioclasts to produce peloids. Scholle (2002) and Scholle and Ulmer-Scholle (2003) described micritization as a diagenetic process through:

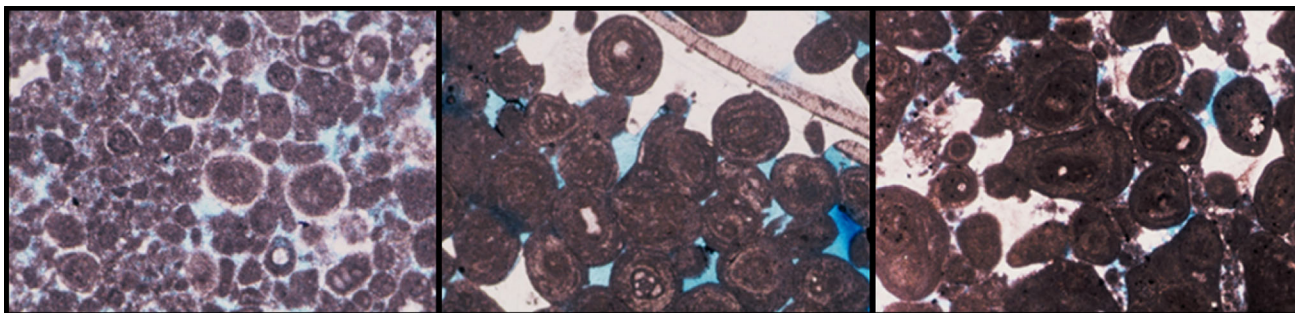


Fig. 5 Different cementation intensities and cement types: calcite fringe rim around grains (left), epitaxial (middle), sparry calcite (right)

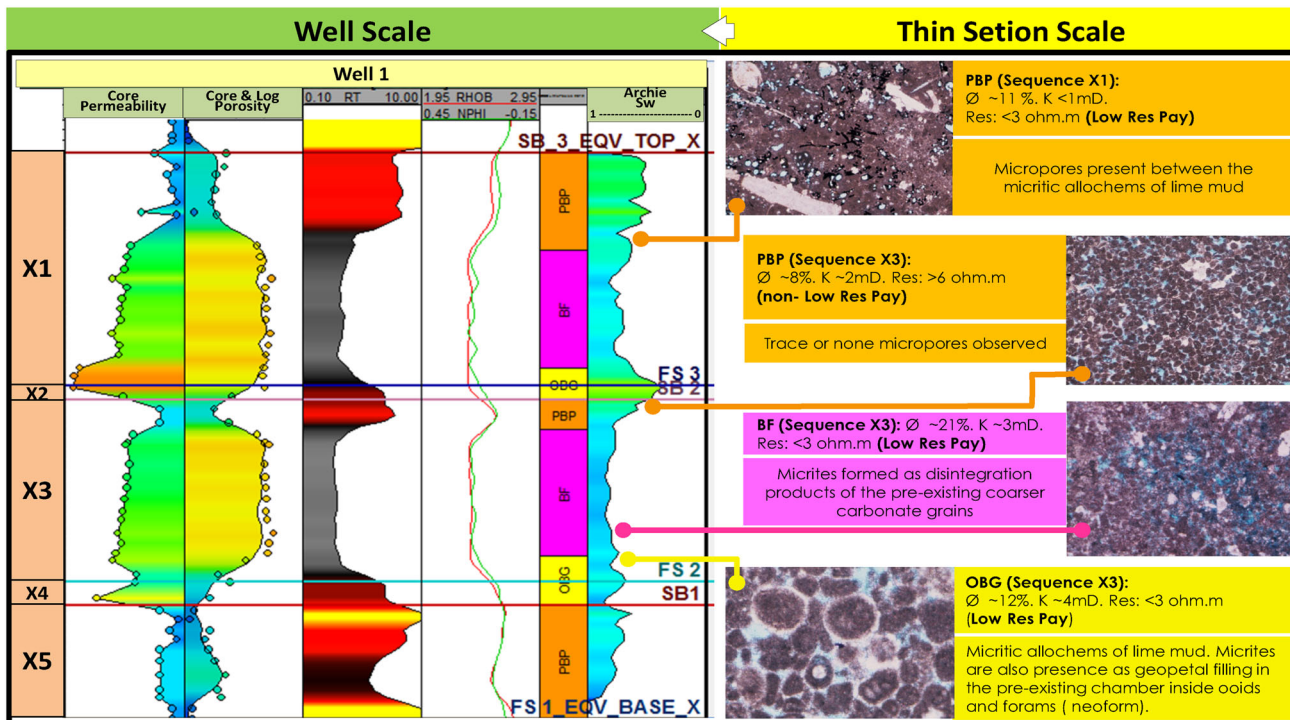


Fig. 6 Vertical distribution of LRP intervals and micropores presence as seen from thin sections. The micropores were present between (1) the micrites of carbonate lime mud (yellow arrow), (2) fine-grained calcite as the result of microborings from calcareous sponges

of coarser carbonate organisms (orange arrow), and (3) neoform fine-grained calcite existing as geopetal filling in the preexisting chamber inside ooids and forams (red arrow)

- its association with microbial metabolism,
- microborings from calcareous sponges of coarser carbonate organisms (grains or skeletal),
- reworked particles,
- altered or neoformed,
- formation of direct inorganic precipitation, or
- precipitation during the long diagenetic history that accompanied burial.

In our study, the formation of micrites and micritized grains led to the deterioration of rock properties by filling the original relatively larger pore space of the rock. As the

amount of micrites increased, the originally larger pore space began to partially or fully occupy and subsequently creating micropores.

Detailed thin section observations from studied reservoir (Figs. 6, 9) showed that these micropores were present between:

- the micritic of carbonate lime mud
- fine-grained calcite as the result of microborings from calcareous sponges of coarser carbonate organisms
- neoform fine-grained calcite existing as geopetal filling in the preexisting chamber inside ooids and forams.

Further evaluation conducted by integrating various dataset including routine core analysis, facies description, thin section, and petrophysical logs revealed that:

1. Micrites and micritization in the studied reservoir occurred on all the identified facies. This suggested a long diagenetic history as early as during deposition and as late as during late burial compaction.
2. High contents of micritic and micritized grains quite aligned with the low-resistivity response. It was therefore reasonable enough to conclude that the vertical distribution of LRP seen on well logs was as a result of vertical variation of micrites and micritized grains and their history over geological time.
3. A specific facies in a particular depositional sequence contained a large amount of micrites that in contrast had undergone less intense micritization during other depositional sequences. For instance, PBP facies that was deposited during sequence X1 at Well-1 was micropores-rich as a result of high contents of micrites. On the other hand, OBG facies that was deposited during sequence X3 at same Well-1 was micropores-rich as a result of neofine-grained calcite existing as geopetal filled in the preexisting chamber inside ooids and forams.

This interesting phenomenon could be explained using sequence stratigraphic concept, which was merely

based on relative sea level and creation/destruction of accommodation space at a particular geological depositional time. Intense micritization occurred on facies that deposited relatively far below the low tide position. In contrast, relatively less intense micritization took place in the area close to the low tide as the energy at this level was strong enough to avoid intense micrites deposition (Fig. 7). This suggests that PBP facies in sequence X1 was deposited in the deeper part of the inner lagoon. Contrarily, PBP facies in sequence X3 was deposited in the shallower part of inner lagoon. Another example is OBG facies in sequence X3 at Well-1 which was deposited in the deeper part of shoal, while OBG facies in sequence X4 at Well-4 was deposited in the shallower part of shoal close to the low tide (Figs. 7, 8).

4. Aerial distribution of the LRP intervals (Fig. 8) showed lateral changes which suggested that the micrites and micritization process that took place in this reservoir occurred with different intensities over geological time. For instance, PBP facies in the upper part of sequence X1 at Well-8 has a relatively higher resistivity response compared to the other wells. Likewise, for OBG facies in sequence X4 at Well-8 with true resistivity reading of around $10 \Omega\text{-m}$ suggested that it was deposited in the shallower part of

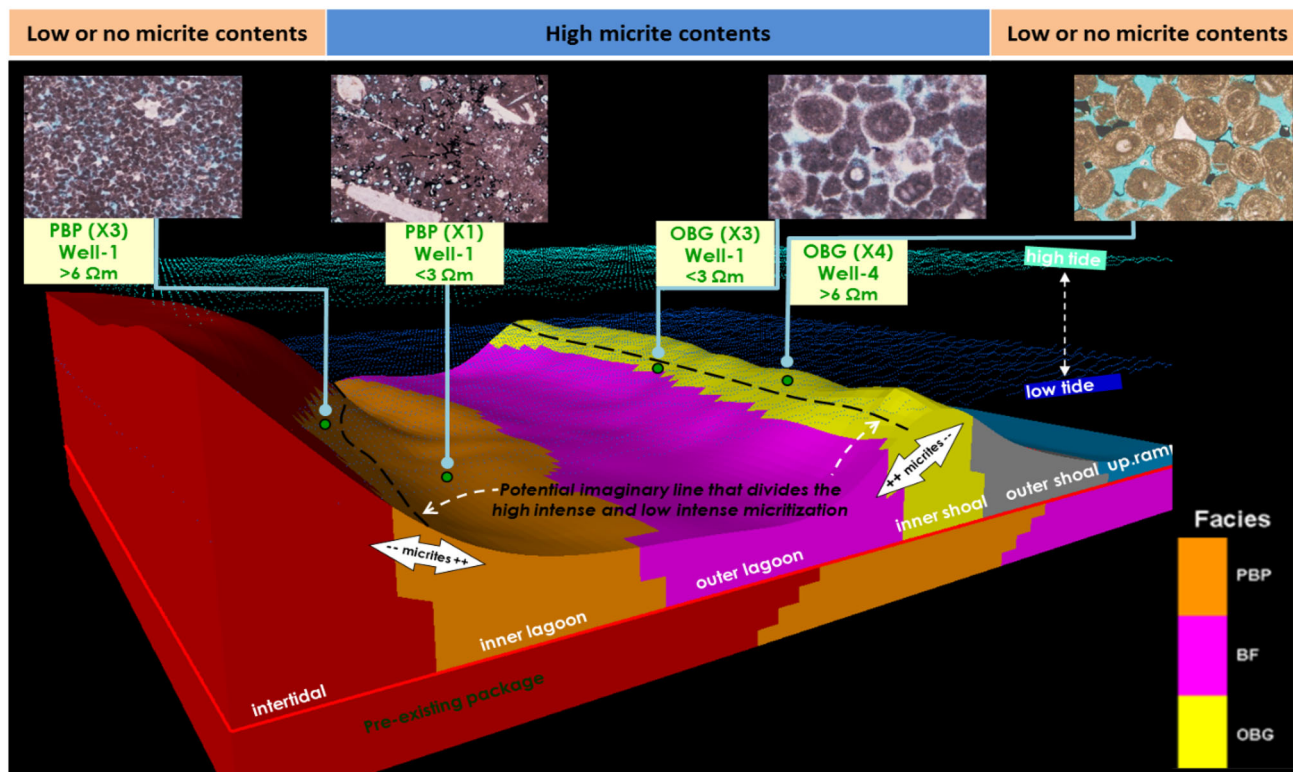


Fig. 7 Geological control for the spatial distribution of micrites intensity

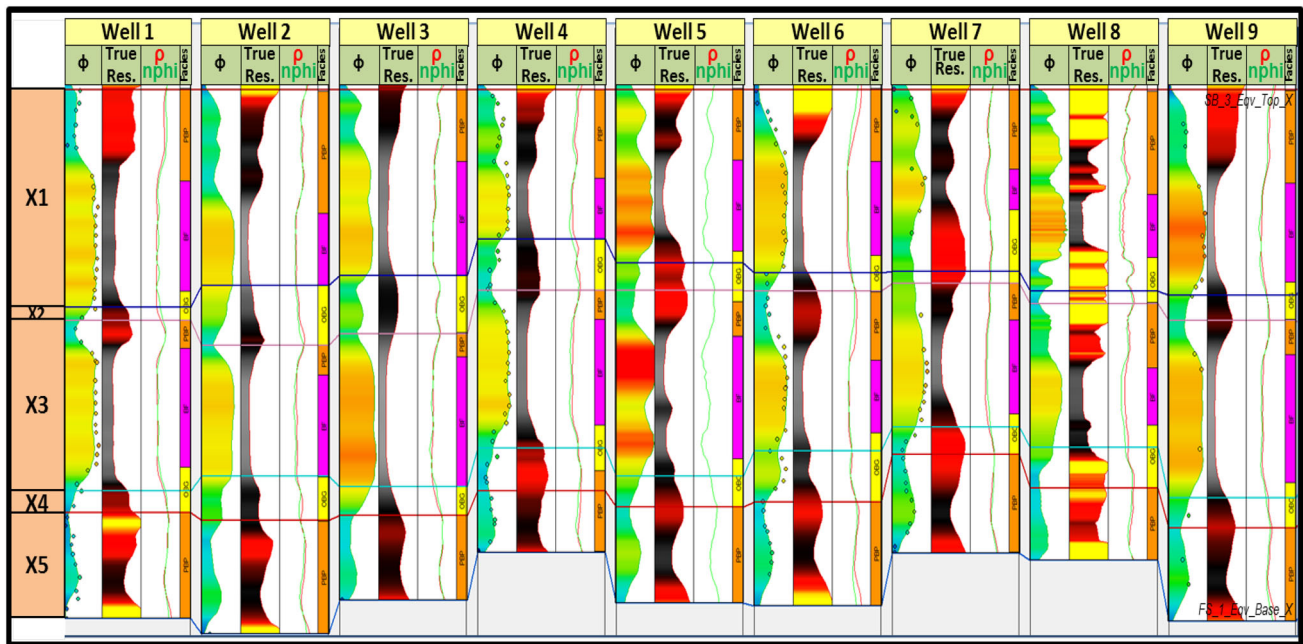


Fig. 8 Stratigraphic cross section (flattened at Reservoir Top) showing vertical and aerial distribution of low-resistivity pay interval on some key wells

inner shoal close to the low tide level. This observation aligned with sequence stratigraphic concept where there is a strong connection between accommodation space and micrites and/or micritized grains abundance at a particular depositional time. Further analysis of the LRP spatial variation in the future would be beneficial for predicting relative sea level depth, depositional environment, and facies distribution in three-dimensional earth model.

Petrophysical and dynamic interpretation

The reservoir was divided into five units as displayed in Fig. 8. The wells in the reservoir were drilled with saline water base mud (WBM) traced with deuterium oxide, as such 15% of the wells were cored and logged with triple combo (bulk density, neutron porosity, and resistivity) tools. The initial petrophysical interpretation was carried out using these conventional logs. Porosity was interpreted from neutron density cross-plot, while the fluid saturation was computed using Gus Archie’s method (Archie 1942). The computed log saturation showed high water saturation; however, other data indicated the presence of hydrocarbon (e.g., mud logs and pressure gradient). Core analysis identified significantly lower water saturation compared with the log analysis (Fig. 9).

Reservoir fluid saturation can be either measured directly in the laboratory using preserved core plug

samples (Dean and Stark 1920), or indirectly by measuring the electrical conductivity of the pore volume, using models such as Archie using resistivity logs, or through the use of PNC logging (Berg 1989). Saturation from Archie is computed using the following equation:

$$S_w^n = \frac{R_w}{\phi^m R_t} \tag{1}$$

where ϕ is porosity, S_w is water saturation, R_w is formation water resistivity, R_t is true formation measured resistivity, and m and n are Archie exponents.

The Archie model considered the following factors, that if not met, the resulted water saturation may not be representatives:

- The presence of conductive minerals (matrix), e.g., clay, pyrite.
- Beds thinner than the logging tool resolution.
- Fresh formation water or the variability of formation salinity
- Reservoir complexity, variation in pore sizes, vugs, fractures.
- Wettability variation.

Archie is only valid when the rock is water wet and free of clay with a uniform pore size distribution (Talabani et al. 2000). Archie equation parameters (a , m , n) are functions of electrical tortuosity, which is related to the pore geometry and wettability (Talabani et al. 2000). Carbonates are well known with their complex pore geometry and varying wetting characteristics, resulting in variations of the Archie

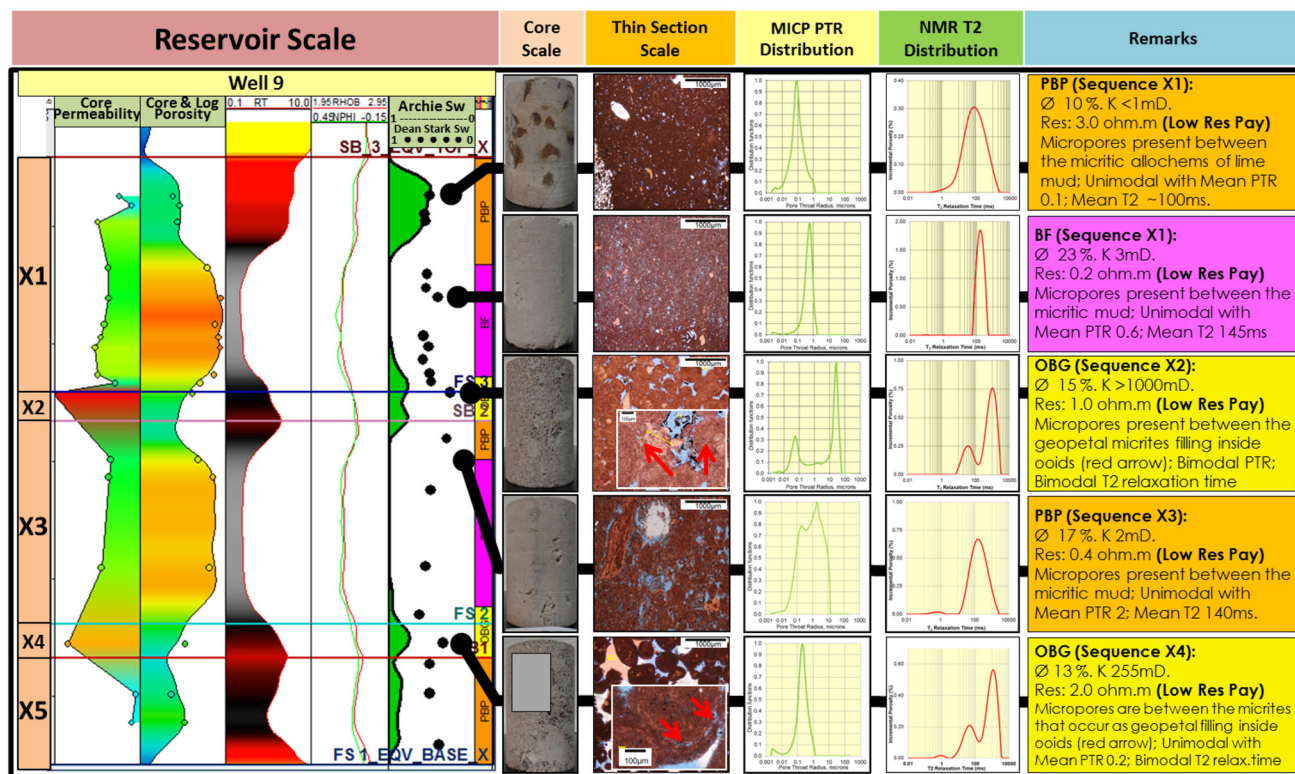


Fig. 9 Integrated analysis on the micropores presence based on well log, thin section, MICP pore throat radius, and NMR pore size distribution from Well-9

exponents across the reservoir. For instance, Bussian (1982) discovered that Archie exponent (a) deviates from an assumed value of one in low-resistivity formations, and same applies to the other two Archie exponents. Thermal neutron capture cross section (Σ log) is an alternative source to evaluate formation water saturation and measures the rate of capture of thermal neutrons in the formation after the emission of high-energy neutron by the tool. The response of the tool is primarily driven by chlorine ion present in the saline formation water, which means the Σ log also known as PNC log delivers saturation that is not conductivity-based. However, the tool has a short depth of investigation and as well can be influenced by mud invasion and the presence of high saline capillary bound water (high chlorine) in micropores. For a mud-invaded interval, the Σ log would only derive valid saturation soon after the mud dissipates which might take years (Khan et al. 2016). For this study, the calculation of water saturation using Σ log was done using Eq. 2 with known formation water salinity (Crain 2006):

$$S_w = \frac{(\Sigma_{LOG} - \Sigma_M) - \phi(\Sigma_H - \Sigma_M)}{\phi(\Sigma_W - \Sigma_H)} \quad (2)$$

where ϕ is porosity, Σ_{LOG} is formation sigma capture cross-section log reading, Σ_M is matrix sigma capture

cross-section log reading, Σ_H is hydrocarbon sigma capture cross-section log reading, Σ_W is formation water sigma capture cross-section log reading

Σ log was acquired for Well-3 once and Well-1 twice, each taken within two years interval. Figures 15 and 16 show the water saturation comparison between resistivity-based and Σ log. Σ log of X3 interval in Well-1 showed low water saturation compared to conventional resistivity-based water saturation. This Σ log measurement was taken 2 years after the start of production, and it indicated the influence of deep mud invasion on the resistivity log. Dean–Stark analysis was conducted on the cores obtained from cored wells to further provide additional water saturation measurements. This method uses distillation extraction by vaporizing the formation water in the core sample using boiling solvent, where both fluids condensed, and water is collected in a calibrated chamber to extract the oil. Then, weight loss is calculated as the difference between the weight before and after extraction, and the water saturation is estimated from the volume of water removed the core sample.

Dean–Stark analysis was carried out on Well-7 and Well-9. These analyses were the only direct saturation measurement approach used in this studied reservoir.

Water saturation of the wells from the Dean–Stark analysis is shown in Figs. 9 and 16 as black dots, and it showed lower water saturation than resistivity-based saturation. The comparison between resistivity-based saturation and core-measured saturation confirmed that the resistivity-based saturation undermined reservoir potential. Meanwhile, the porosity computed from the log and core perfectly matched for both wells. However, the core from tight intervals could give inaccurate saturation because of the tendency to prematurely terminate the distillation process due to the low rate of water recovery, under the assumption that the process was over (Dandekar 2013). Hence, it is possible for Dean–Stark analysis to undermine the water saturation in a tight reservoir. This case is shown in Fig. 16 for Well-7 in X5. Therefore, the discussion in this study focused on Dean–Stark analysis was in relation to the good quality rock interval. Thus, the interpreted high water saturation from resistivity log is observed to be a result of either or a combination of:

- Deep mud invasion as a result of overbalanced drilling using high saline mud.
- Presence of microporosity and conductive bound water.
- Presence of metallic minerals (e.g., pyrite).

Core analysis

Routine core analysis, MICP, and NMR measurements were taken for all the cores. Petrophysical groups (PG) were identified based on the core analysis (MICP data). Figure 10 is a cross-plot of permeability and porosity, capillary pressure, and pore throat radius (PTR) distribution. From the Figure, PG-7 (green color) showed the best rock properties (high permeability and porosity and low entry capillary pressure), with dual pore system as seen in the PTR distribution, while PG-1 (yellow color) showed the poorest rock properties—low permeability and porosity and high entry capillary pressure, with single pore system

as seen in the PTR distribution. NMR measurement was taken on selected core plug samples to further identify the different pore systems. The basic principle of NMR measurements is that it directly relates the generated echo decay sequences or relaxation time to the pore size distributions (PSD). The NMR signal detected from core plug has T_2 components for every different pore size in the core. Then, these components can be extracted from the total NMR signal to form T_2 distribution using mathematical inversion. This distribution is effectively the pore size distribution, which can infer various petrophysical parameters such as porosity, permeability, and free and bound fluid ratios. Figure 9 shows the T_2 distribution for five different core samples across the interval of Well-9 and the T_2 cutoff in the case of dual pore system ranges between 120 and 150 mS to separate microporosity from macroporosity.

Figure 9 shows an integrated analysis of the presence of micropores based on the well log, thin section, MICP, and NMR from Well-9. Thin section from five different samples across the interval displayed the presence of micropores between micritic materials as discussed earlier. This is then further supported by MICP result that showed low PTR value of 0.01 to 1 microns that mostly exist in the poor rock quality. The good rock quality showed a bimodal distribution comprised of low PTR and high PTR (>10 microns), but majorly dominated by the high PTR. NMR pore size distribution showed a similar trend to the MICP distribution, although the two measurements assessed the same pore space but in a different manner. The difference is that in the MICP case, injected mercury moved through the pore throats while for NMR, the magnetized decay probed the pore volume. Likewise, MICP measurements were taken on a chip of rock sample, which assessed a little portion of the rock, while NMR measurements were taken on the whole core plug. Bound and mobile phases were clearly identified from the NMR T_2 spectrum as well from the MICP on the same sample with dual pore system.

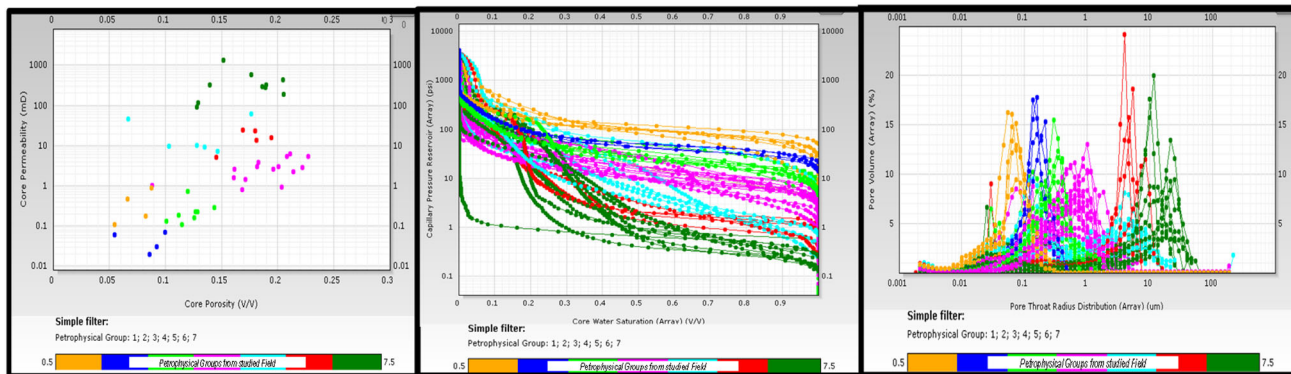


Fig. 10 Seven identified petrophysical groups based on porosity–permeability, capillary pressure–water saturation, and pore throat radius distribution

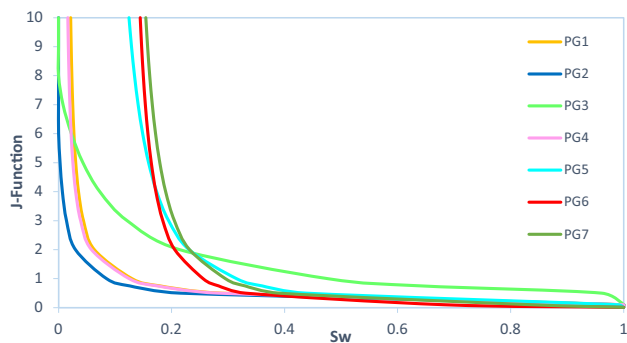


Fig. 11 Leverett J -function from MICP rock-typed specific used to developed the saturation height modeling

The saturation model for each PG was developed from MICP data using the Leverett J -function (Eq. 3) by taking into consideration the FWL interpretation. The J -function curve was employed to correlate capillary pressure–water saturation data for core samples with similar pore types and wettability (PGs). On plotting the J -function against the wetting phase saturation, it was found that all the data points fell roughly along the same trend. Hence, the J -function curves were normalized for each PG with power equation to obtain single J -function for each particular PG as shown in Fig. 11. The J -function for each PG was converted back to capillary pressure in order to generate the modeled saturation height functions by subtracting the FWL and the division of the capillary pressure and water–oil pressure gradient difference.

$$J(S_w) = \frac{0.217P_c}{\sigma \cos \theta} \sqrt{\frac{k}{\phi}} \quad (3)$$

Special core analyses (SCAL) were carried out on Well-9 from Area B. The measurements included porous plate capillary pressure and centrifugal water–oil capillary pressure. The information gathered from these sources was used in establishing capillary pressure saturation modeling for the dynamic simulation model input. The selected cores from various PGs that showed similar capillary pressure trend were grouped accordingly into three groups. Figure 12 shows the model capillary pressure where PG_HIGH represented PG-6 and PG-7, PG_MED represented PG-3, PG-4, and PG-5, while PG_LOW represented PG-1 and PG-2.

Wireline formation testers and production tests

Given the limitations of the resistivity-based interpretation approach, another alternative was to use pressure gradient profiles to confirm the presence of hydrocarbon and determine the fluid contacts. Pressure points acquired across the formation interval using wireline formation

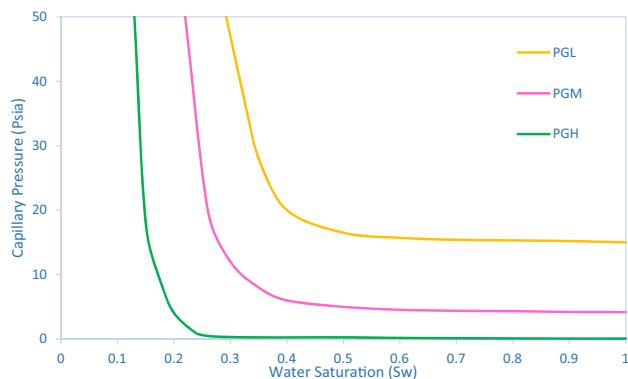


Fig. 12 Model capillary pressure–saturation obtained from porous plate/centrifuge

testers were gathered from different wells. The results are plotted in Fig. 13 for Area A and Fig. 14 for Area B.

In Area A, Well-1, Well-3, and Well-13 showed an average oil pressure gradient of 0.342 psi/ft., while Well-2, Well-4 and Well-14 showed an average pressure gradient of 0.49 psi/ft. considering formation water salinity of 200,000 ppm. Well-15 pressure points deviated from other points due to pressure depletion that occurred over time in the area; however, an oil pressure gradient of 0.34psi/ft. was obtained. This showed completely oil zone in the interval between XX25 and XX50 and completely water zone below XX75. Thus, the interval between XX50 and XX75 showed a clear indication of the transition zone, and the free water level (FWL) was better positioned by considering production tests data (Fig. 13). DST from Well-1 and Well-3 at the interval (XX25 and XX50) produced oil with 0–3% water cut. Well-1 was placed on production across this interval and produced oil with only about 5% water cut till date. Test carried out in the interval between XX50 and XX75 produced almost 100% water for Well-2 and Well-13. Combining the possible cross-over of the oil and water pressure gradient with the production tests gave the confidence of placing the FWL at the midpoint between XX50 and XX75 with an uncertainty of ± 10 ft.

In Area B, Well-5, Well-6 (upper pressure points), and Well-10 showed an average oil pressure gradient of 0.3 psi/ft. which indicated that interval between XX80 and XX120 was located in the oil zone. Upper pressure points of Well-9, which were taken after little pressure depletion, showed an oil pressure gradient of 0.32 psi/ft, while lower pressure points of Well-6 and Well-9 showed a water pressure gradient of 0.49 psi/ft. Because not many pressure points were taken below XX120, uncertainties ensued. But combining the points with test data helped us to better position the FWL. Similar to what was mentioned in Area A, Well-5, Well-11, and Well-12 produced a thousand barrels of oil

Fig. 13 WFT pressure points and production test for Area A

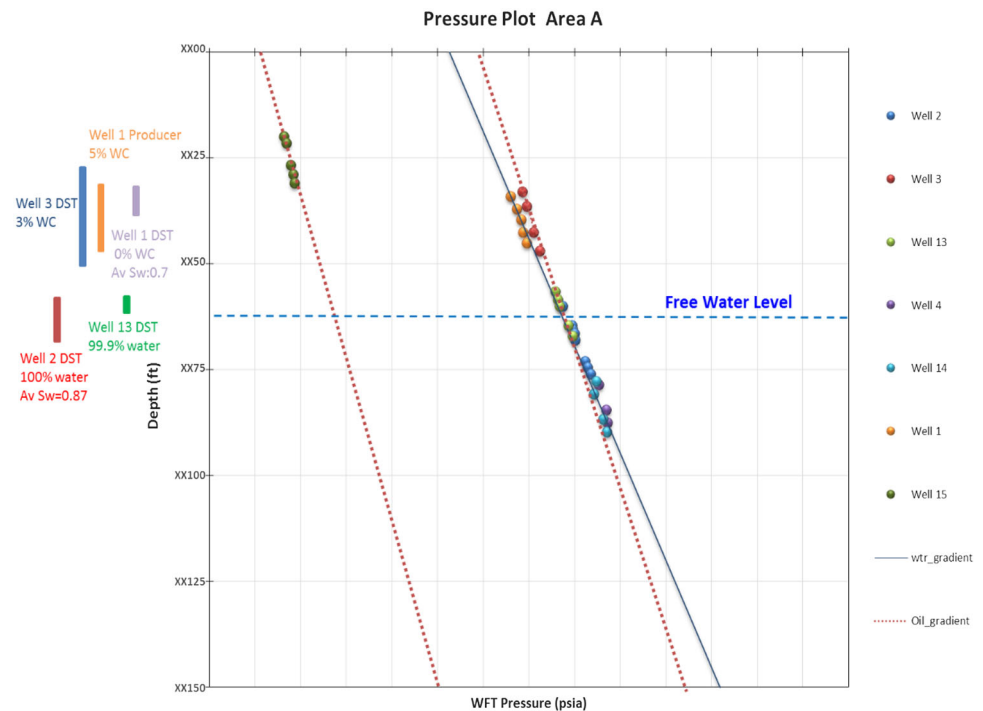
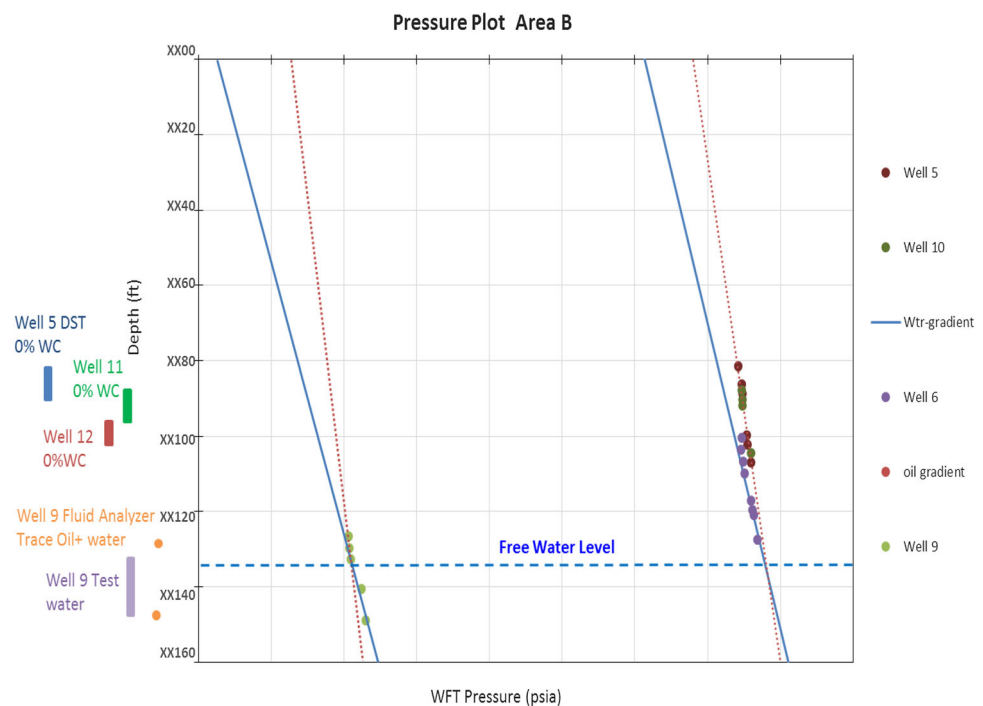


Fig. 14 WFT pressure points and production test for Area B



with no water cut and supported the fact that XX80–XX120 was located in the oil zone. Fluid analyzer coupled with WFT in Well-9 showed water with a trace amount of oil, while production test produced 100% water. Then, the FWL was observed to lie in the interval between XX120 and XX140 and selected close to XX140 due to more uncertainties around this interval.

Data integration

One of the main tasks was to build a saturation model for hydrocarbon volume calculation and field development study. The resistivity-based saturation log exhibited a water zone. Integrating several approaches to model the water saturation was required since the problem was actually

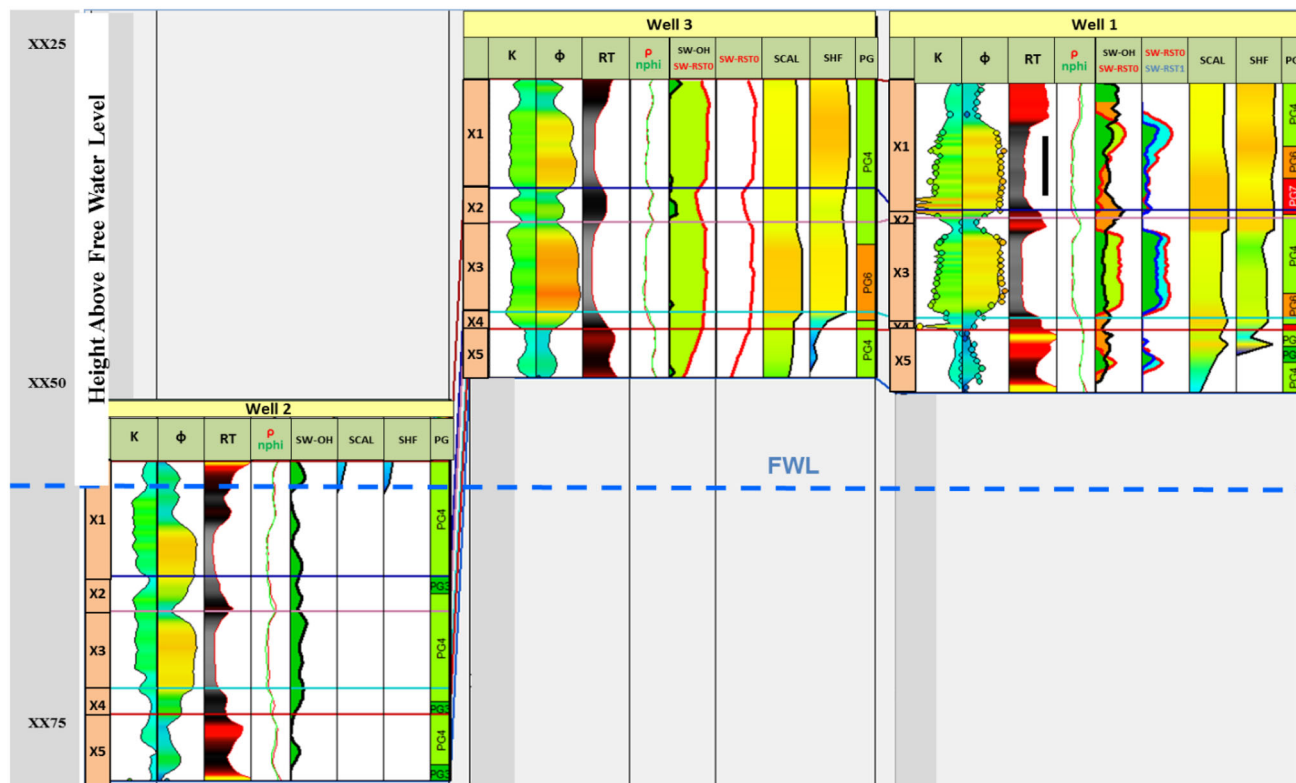


Fig. 15 Structural well correlation comparing all saturation-based methods in Area A. Track 1 log and core permeability with scale 0.01–1000 mD from right to left. Track 2 log and core porosity with scale 0–0.30 from left to right. Track 3 horizontal resistivity with scale 0.1–20 Ω -m from left to right. Track 4 density neutron log. Track 5 open-hole saturation based on Archie compared with sigma

log at initial time with scale 0.0–1.0 from left to right. Track 6 saturation comparison between initial sigma log and the final sigma log with scale 0.0–1.0 from left to right. Track 7 model saturation based on SCAL data input with scale 0.0–1.0 from left to right. Track 8 saturation height model based on MICP data input with scale 0.0–1.0 from left to right. Track 9 petrophysical group

related to the structurally parallel FWL based on the log. Figures 15 and 16 show the comparison of various saturation calculation approaches which was discussed earlier based on well correlations. Figure 15 shows the comparison between Well-2, Well-3, and Well-1 in Area A, and Fig. 16 shows the comparison between Well-6, Well-7, and Well-5 in Area B.

Critical evaluation of the interval between XX25 and XX50 (which showed oil interval from WFT and test data analysis) on electrical log showed low resistivity. The crestal wells (Well-3 and Well-1) in Area A have similar rock characteristics as seen in Fig. 15. The resistivity from X1 and X3 with very good rock properties (PG4–PG7) was low, which indicated an overestimation of the water saturation. Comparing saturation from Archie with the one from Sigma log taken 2 years after the convectional logging in Well-1 showed that there was mud dissipation and oil reoccupation of the vacant pores. The Sigma log taken 4 years later confirmed the oil movement during production. The water saturation from Sigma log indicated that the zone of interest contained 20–25% water saturation which confirmed the core interpretation.

Saturation height model from MICP showed a good oil saturation which is consistent with the sigma-based saturation. Capillary pressure–saturation relationship derived from SCAL showed a very good consistency with the aforementioned methods. This gave the confidence that the interval between XX25 and XX50 is an oil interval, and its evaluation based on resistivity-based method was inaccurate. Below XX50 in the transition zone, above the selected FWL, the three approaches showed consistent result aside the resistivity-based method. Another interesting note was that the resistivity-based method in Well-2 showed average saturation of 80% below the FWL, whereas during testing 100% water was produced. Hence, the oil observed in the resistivity-based method could represent the residual oil saturation.

Well-5, located on the crestal part of Area B, showed low resistivity on X1 and X3 layer though the well has very good rock properties (PG4–PG7). In the above discussion, XX80–XX120 was identified as an oil zone which produced oil with trace or no water. The saturation from resistivity-based method overestimated the water saturation, while saturation from MICP and SCAL was consistent. Well-7 showed good consistency around this interval between resistivity-based

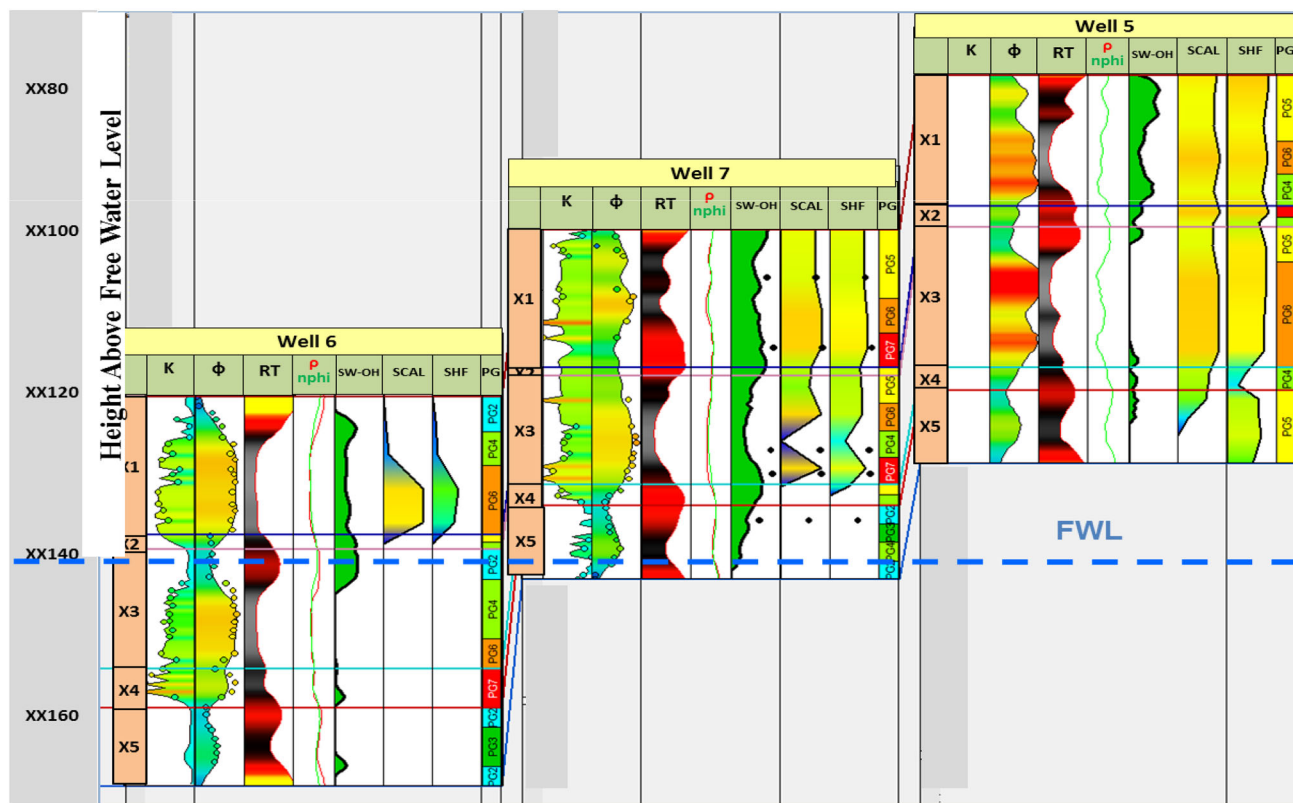


Fig. 16 Structural well correlation comparing all saturation-based methods in Area B. *Track 1* log and core permeability. *Track 2* log and core porosity. *Track 3* horizontal resistivity (black) was used as R_t for saturation computation in conventional analysis. *Track 4* density neutron log. *Track 5* open-hole saturation based on Archie compared

with saturation from Dean–Stark (especially for Well-7). *Track 6*: model saturation based on SCAL data input compared with saturation from Dean–Stark (especially for Well-7). *Track 7*: saturation height model based on MICP data input compared with saturation from Dean–Stark (especially for Well-7). *Track 8*: petrophysical group

method, MICP, SCAL, and Dean–Stark. The observed FWL was also justified with the consistency between all the approaches in the interval between XX120 and XX160.

Finally, data integration of the above showed that saturations based on Archie are prone to higher uncertainties if compared to those derived from the MICP, Sigma log, Dean–Stark, and SCAL, in the pay intervals, due to a relatively low resistivity measured by the electrical log. Choosing one method of saturation, while disregarding the others may not be ideal, on the contrary, integration of more than one method to identify the potential uncertainty range is highly recommended. This interdisciplinary study was carried out using the workflow presented in Fig. 17. There are significant differences in hydrocarbon volumes calculated from the different methodologies, which was as much as five times the original volume.

Validation and implementation

Having identified the presence of LRP reservoir, and the discrepancy between resistivity log data and other sources like core, pressure, and DST results, a low confidence was

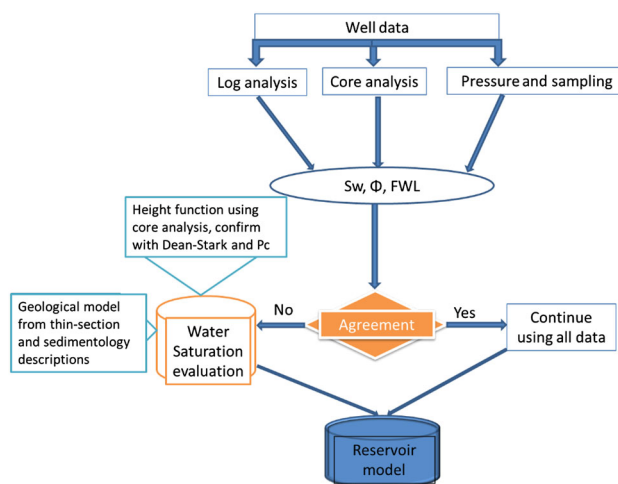


Fig. 17 Interdisciplinary study workflow

placed on the calculated saturation from the resistivity. Hence, the field simulation model was developed based on the saturation height function that honored SCAL, well test, Dean–Stark and formation pressures, considering the newly derived FWL. The old simulation model was based

Fig. 18 Comparison between old (*left*) and new (*right*) model water saturations. The color gradient variation is from *deep blue* to *deep red* with *blue* representing water and *red* representing oil

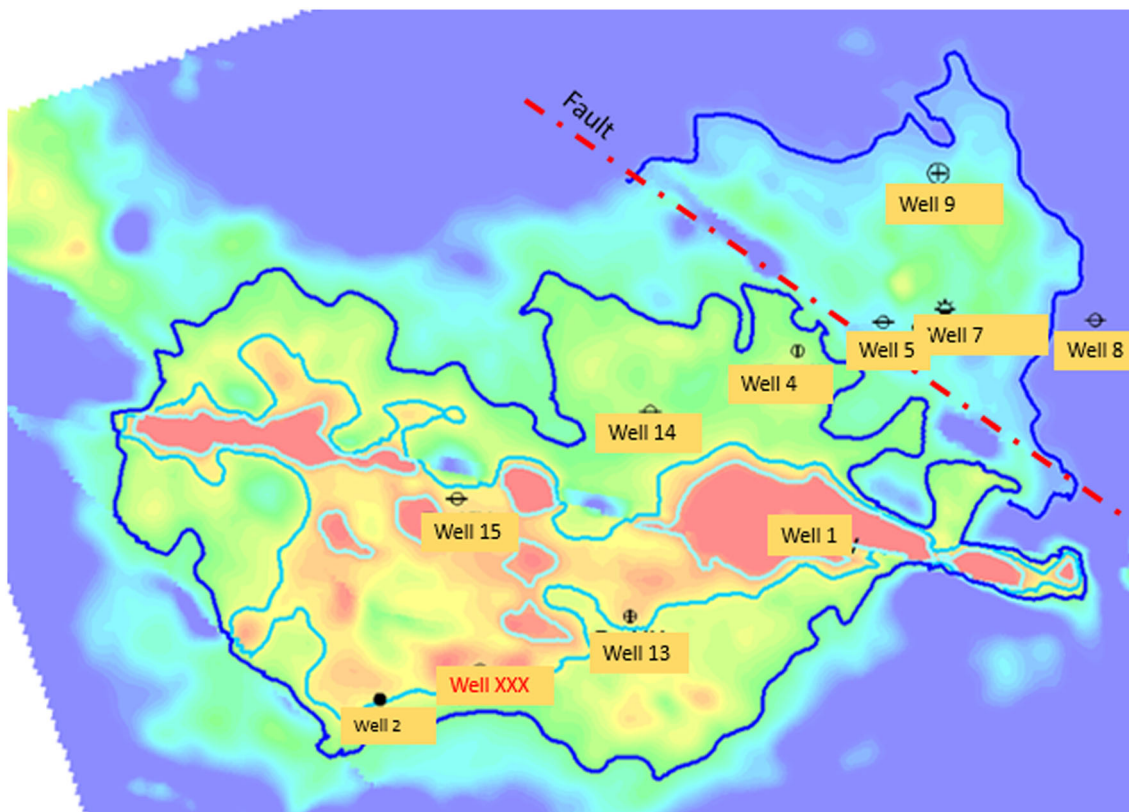
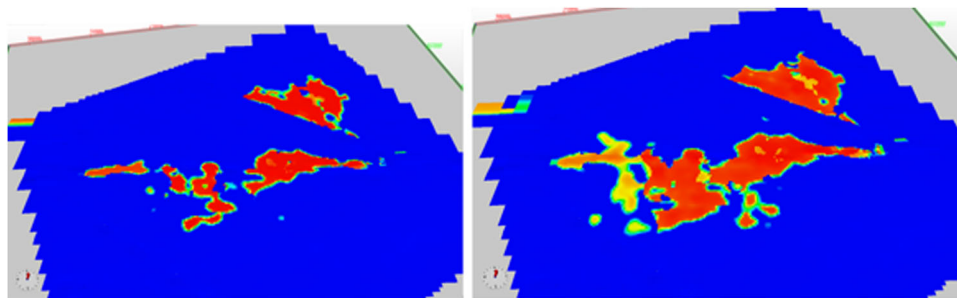


Fig. 19 Illustration of the reservoir map showing the old FWL (*light blue*) and the new FWL (*dark blue*). Well XXX is below the old FWL and close to the newly defined FWL

on the FWL assessment found on the logs, which did not consider integrating all available data. The old model simulated a shallower oil water contact (OWC) and a small oil pool as seen in the comparison between old and new model in Fig. 18. The new model displayed a higher oil saturation as compared to the old model, resulting in a higher stock tank oil in place (STOIP).

The results of the simulation model indicated that oil was present in intervals regarded as water zone. Hence, we attempted to validate the model by drilling a new well (XXX) in Area A close to the newly defined FWL and below the previous FWL toward the southeastern part of the reservoir (Fig. 19). The location of well XXX was found as 100% water based on the old simulation model,

being so close to old FWL. However, the new model showed deeper FWL.

The data acquisition for well XXX consisted of triple combo, NMR, and traced coring. Logging was done on LWD after cutting core across the reservoir to reduce the influence of mud invasion on resistivity reading. The well was drilled with water base mud (salinity of 200,000 ppm) traced with deuterium oxide for saturation determination. Figure 20 illustrates the acquired data. Despite using LWD, the resistivity across the reservoir was still low and varied between 0.3 and 0.4 Ω -m. These low values indicated no hydrocarbon across the interval, which implied that this interval is 100% water bearing. The NMR log profile showed unimodal pore system, with little

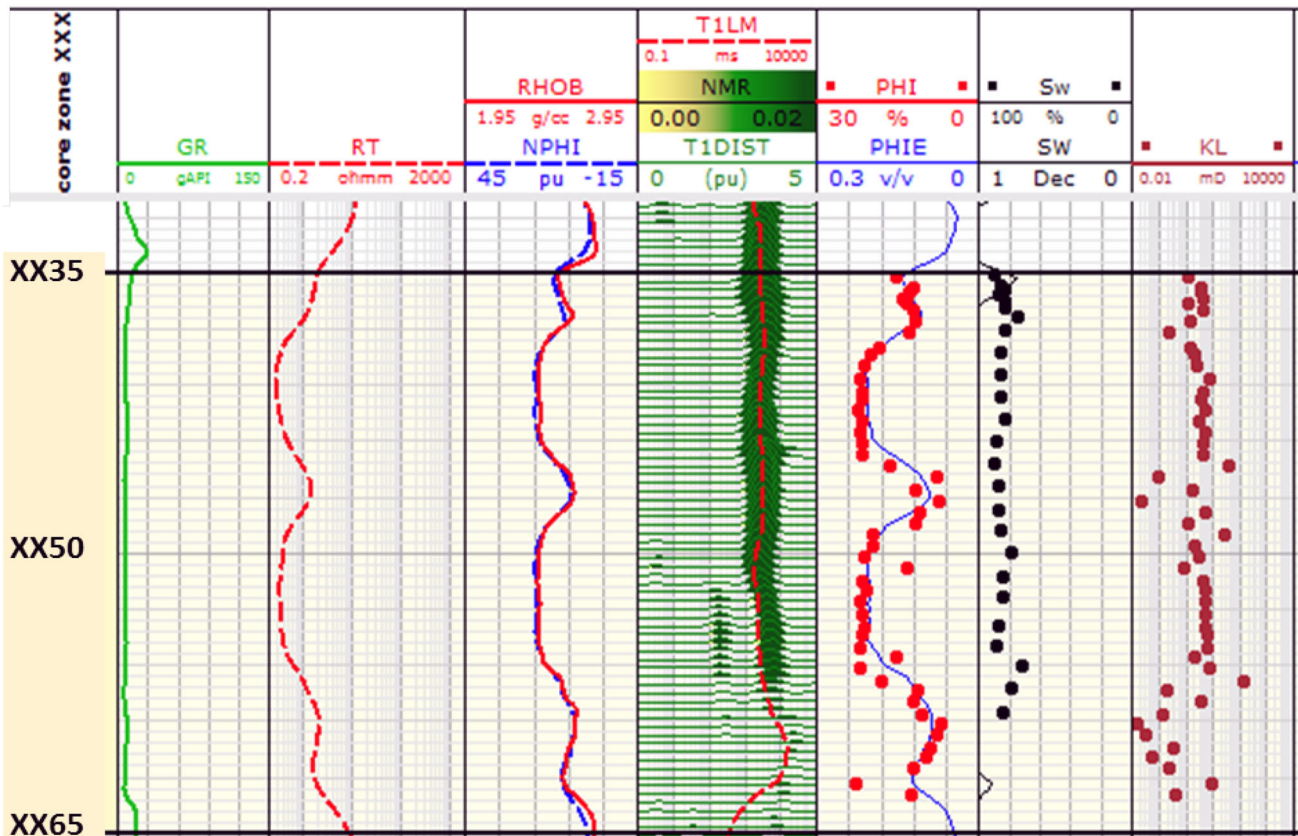


Fig. 20 Well XXX acquired log analysis. *Track 1:* coring interval. *Track 2:* gamma-ray reading. *Track 3:* deep resistivity. *Track 4:* density and neutron porosity. *Track 5:* NMR distribution. *Track 6:*

log-calculated and core-measured porosity. *Track 7:* log-calculated and core-measured water saturation. *Track 8:* core-measured permeability

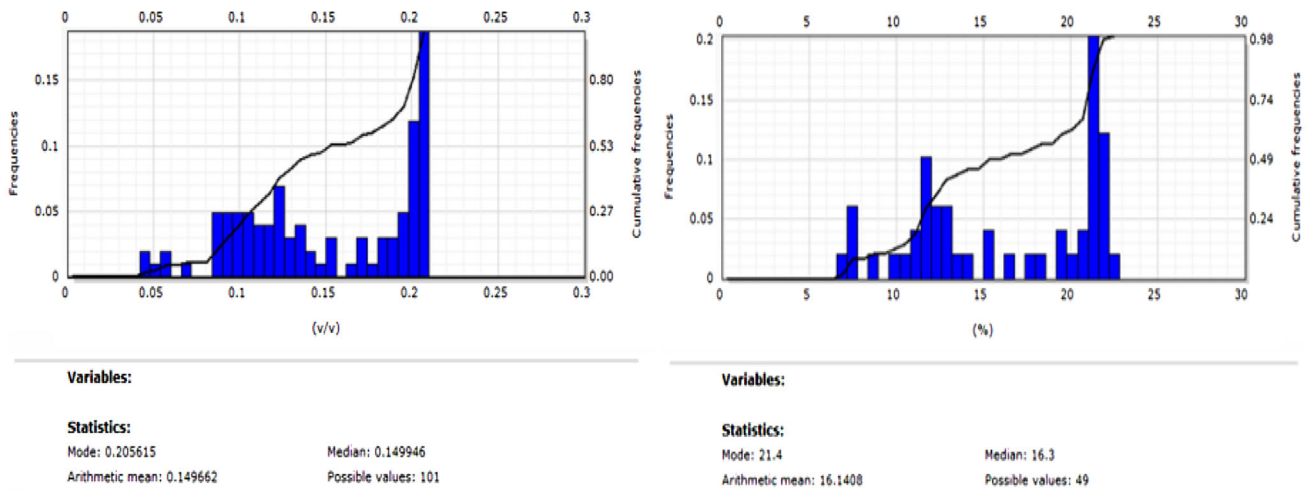
fluctuations reflecting homogeneous properties with single pore space. However, within the lower part of the reservoir, NMR indicates a change in the pore size distribution.

Thirty feet of core was cut. The core was traced using a known concentration of deuterium oxide. As soon as the core reached the surface, it was cut to 3 ft. sections, wax preserved, and shipped to the laboratory. Measurements commenced as soon as the core arrived. Plugs were selected to cover the whole reservoir interval. The core plugs for Dean–Stark analysis were cut using liquid nitrogen and the conventional plugs using saline water. Samples were cleaned, dried, and conventional porosity and permeability measurements were taken. Figure 20 shows a comparison between log analysis and core measurements. Core porosity showed an excellent match with the log porosity. The histogram comparing the two data analysis is shown in Fig. 21 and around 1 porosity unit was the difference between the two, which is considered as an excellent match. However, saturation exhibited different results: Dean–Stark analysis indicated an average of 80% water saturation across the interval as compared with 100% water saturation computed from logs. The porosity and permeability distributions across the interval showed good

rock quality, which is advantageous to Dean–Stark analysis as mentioned earlier. The results from Dean–Stark measurement were confirmed qualitatively using Ultraviolet (UV) light on the slabbed core.

Figure 22 shows a slabbed core photograph under normal and UV light, where oil staining is quite noticeable. The two sources of information (UV light and Dean–Stark) verified the presence of hydrocarbon in this reservoir.

Further analysis on the core was performed to evaluate one of the causes of LRP we presented. XRD analysis was performed on selected samples of the core throughout the formation. The result showed a mix of minerals with calcite being the dominant lithology (average 90%), dolomite ranged between 2 and 20%, clay content (1–6%), and worthy of note was 2–4% of pyrite sporadically measured (Fig. 23). Paramagnetic minerals such as pyrite have been identified as one of the causes of LRP. However, it needs to be present in high percentage, i.e., more than 5%, to have meaningful impact on resistivity. Clavier et al. (1976) reported that the effect of pyrite on resistivity logs depends on its electrical continuity, and to provide such continuity, they needed to be in excess of 5%.



Porosity-Log analysis

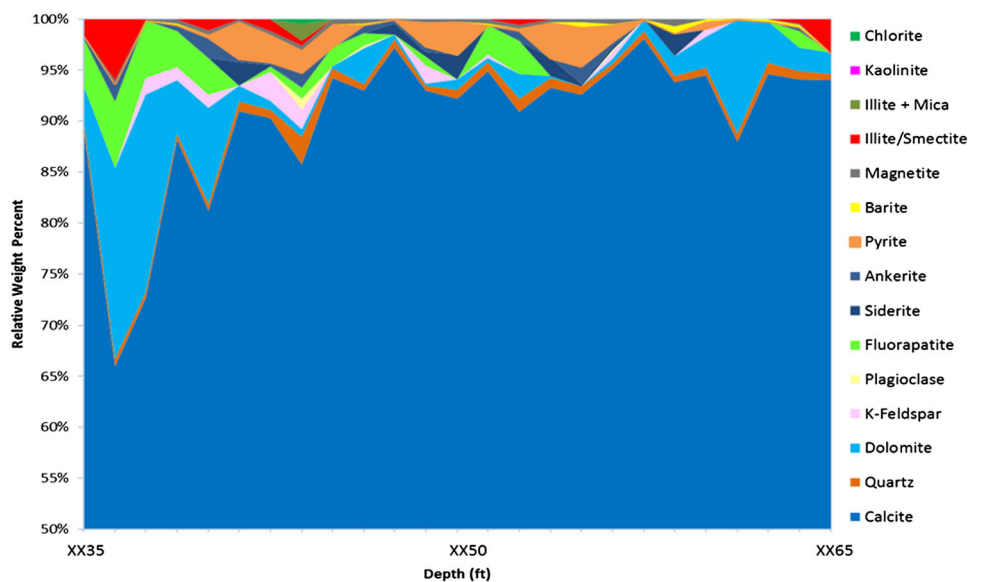
Porosity-core measurement

Fig. 21 Histogram of porosity distribution comparison between log and core measurements

Fig. 22 Well XXX slabbed core under normal light (left image) and under UV light with oil staining (right image)



Fig. 23 XRD results showing the mineral fraction of 15 samples across the formation interval



The acquired NMR log showed a unimodal pore system represented by one peak across the interval aside the lower section as seen in Fig. 20, where a possible dual modal could be interpreted. However, the core NMR response exhibited a different signature. The discrepancy between the log and core NMR could be as a result of the high salinity mud dominating the log NMR signal (Ashqar et al. 2016). This means that the log NMR was responding to the mud rather than the formation pore size, and as a result demonstrated no change of NMR log signal throughout most of the section. Core NMR measurements were taken

on saturated samples. The measurement showed variation in PSD as illustrated in Fig. 24.

The PSD across the formation can be divided into different patterns, which are categorized as follows:

- Samples showing unimodal PSD (Fig. 25a).
- Samples showing bimodal system, these are subdivided into the following.
 - Samples with the pore distribution dominated by the large pores (Fig. 25b).
 - Samples with equal micropores and large pores (Fig. 25c).
 - Samples with the pore system dominated by micropores (Fig. 25d).

The variation in the pore distribution signature shows the complexity of the candidate carbonate reservoir, as such minimum of three/four rock types could be identified from the studied reservoir. The four different PSD show different cutoff between the free and bound fluid represented by the micritic type with the cutoff range between 20 and 170 mS.

Since all intervals producing water-free oil were identified by WFT and further confirmed by production tests, using overestimated water saturation from resistivity-based method in the LRP significantly underestimated reserves.

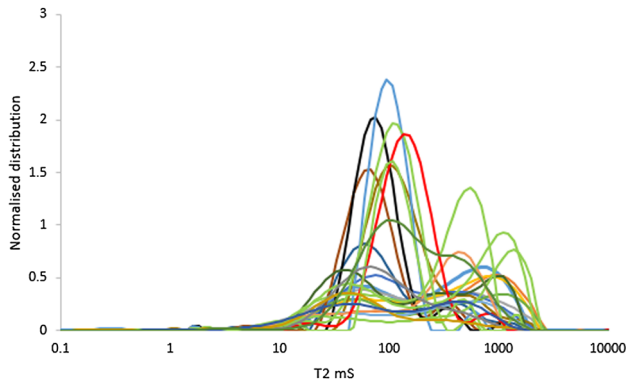


Fig. 24 Core NMR pore size distribution across the reservoir

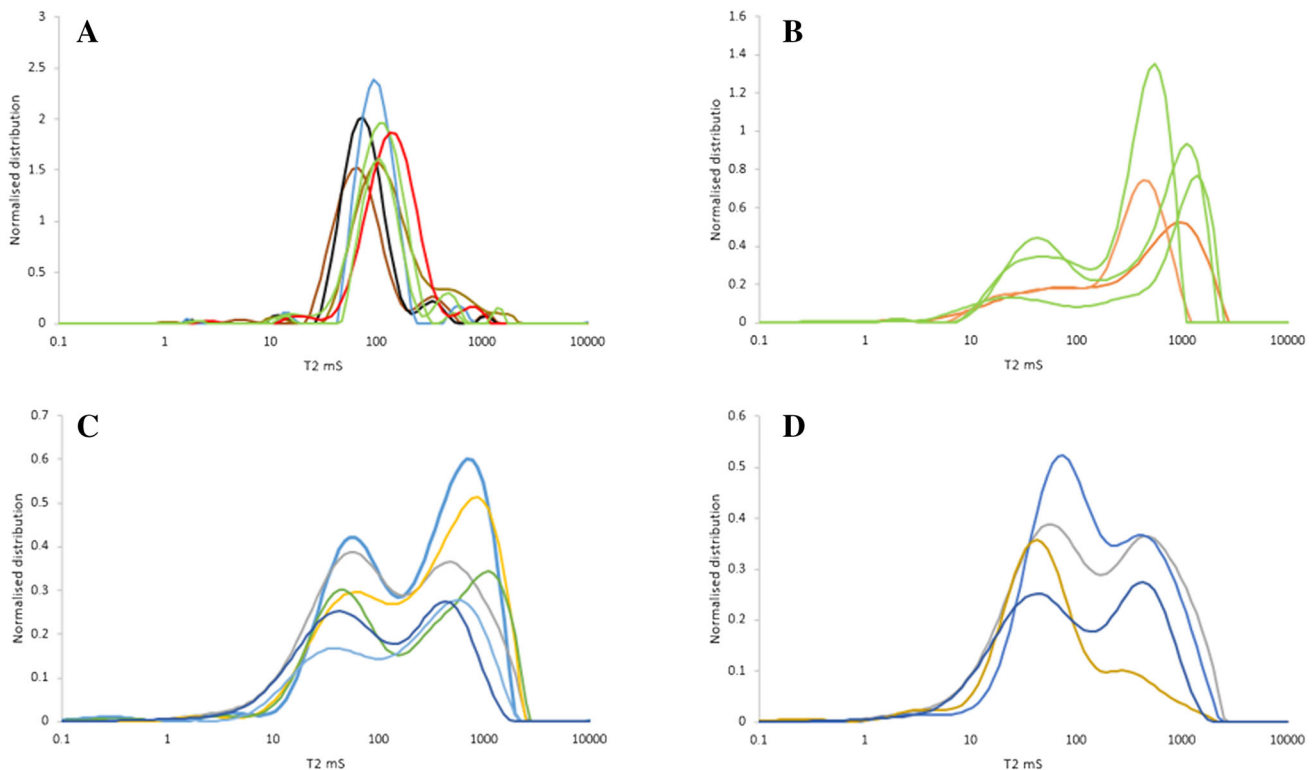


Fig. 25 Core NMR pore size distribution across the reservoir

Consequently, the calculation of STOIP improved drastically when the dynamic model was initialized with the newly derived FWL and saturation height equations (modeled from the capillary pressure dataset). At the same time, updated dynamic simulation model based on new dynamic capillary pressure dataset showed better history matching. The results of the new model were validated with the data acquired from the new well drilled close to the new FWL. The advantage of using such an integrated approach minimizes the error as a result of overestimating water saturation, improves decision in well completion, improves the well performance prediction, and reduces uncertainty in reserve estimation. Saturation profiles derived by this approach can be better fitted due to substantial reduction in uncertainties of resistivity-based saturation data.

Concluding remarks

Based on the results of this work, the following conclusions are drawn:

- The identified probable causes of LRP in the studied reservoir are the existing micropores and deep mud invasion. Though when LWD was used for the new well, the resistivity remained low. XRD showed the presence of less than 5% paramagnetic mineral (pyrite). This low concentration is considered to be of minimal effect on the log resistivity measurements. Hence, presence of paramagnetic materials as the cause of LRP in the candidate formation was discarded.
- The integrated study has shown the effectiveness of saturation height function based on petrophysical grouping from core analysis in mitigating the uncertainties of resistivity-based saturation.
- For LRP reservoir, improving FWL accuracy is critical in the evaluation of the pay zone.
- A robust workflow has been illustrated to evaluate water saturation in LRP. This workflow could be applied to conventional reservoirs.
- Integration of several of these approaches is recommended to capture the potential uncertainty in the water saturation calculation.
- In order to better understand LRP interval, the following should be addressed: multidisciplinary integrated studies and better understanding of the sedimentological and diagenetical process that control the spatial distribution of LRP zone.
- The existence of oil at the new well location was confirmed by fluorescence and Dean–Stark results, though conventional logs showed the well as 100% water. The accuracy of new FWL and new saturation

model was confirmed through the analysis of this cored well. STOIP increased significantly compared with that of the previous model

- NMR logging indicated single PSD, with small variation at the lower part of the reservoir, and this is thought to be a result of the high saline mud masking the NMR formation signal, whereas NMR signal from the core samples showed the presence of microporosity, which sometimes dominates the pore system

Acknowledgements The authors would like to appreciate Abu Dhabi Company for Onshore Petroleum Operations Ltd' management and its shareholders for granting the permission to publish this paper. We would like to thank the reviewers for their valuable comments.

Open Access This article is distributed under the terms of the Creative Commons Attribution 4.0 International License (<http://creativecommons.org/licenses/by/4.0/>), which permits unrestricted use, distribution, and reproduction in any medium, provided you give appropriate credit to the original author(s) and the source, provide a link to the Creative Commons license, and indicate if changes were made.

References

- Archie GE (1942) The electrical resistivity log as an aid in determining some reservoir characteristics. *Pet Trans AIME* 146:54–62
- Ashqar A, Uchida M, Salahuddin AA, Olayiwola S, Awolayo AN (2016) Evaluating a complex low-resistivity pay carbonate reservoir onshore Abu Dhabi: from model to implementation. In: SPE 182912-MS presented at Abu Dhabi International Conference and Exhibition
- Asquith GB (1985) Handbook of log evaluation techniques for carbonate reservoirs. American Association of Petroleum Geologists, Tulsa, OK, United States
- Awolayo A, Sarma H, Al-Sumaiti A (2015) An experimental investigation into the impact of sulfate ions in smart water to improve oil recovery in carbonate reservoirs. *Transp Porous Media* 111(3):649–668
- Berg VD (1989) The capability of pulsed neutron capture logging to determine oil and gas saturations, SPE 19614
- Boyd A, Darling H, Tabanou J (1995) The lowdown on low-resistivity pay. *Schlumberger Oil Field Rev* 7(3):4–18
- Bussian A (1982) A generalized Archie equation. In: SPWLA 23rd Annual Logging Symposium. Society of Petrophysicists and Well-Log Analysts
- Chu W, Steckhan J (2011) A practical approach to determine low-resistivity pay in clastic reservoirs. *Soc Pet Eng. SPE ATCE*. SPE-147360
- Clavier C, Heim A, Scala C (1976) Effect of pyrite on resistivity and other logging measurement, SPWLA Seventeenth annual logging symposium
- Crain ER (2006) Crain's Petrophysical Pocket Pal. ER Ross, Ontario
- Dandekar AY (2013) Petroleum reservoir rock and fluid properties. CRC Press, Boca Raton
- Dean EW, Stark DD (1920) A convenient method for the determination of water in petroleum and other organic emulsions. *Ind Eng Chem* 12(5):486–490

- Dunham RJ (1962) Classification of carbonate rocks according to depositional texture. AAPG Memoir 1:108–121
- Farouk A, Wibowo S, Aillud G, Al Shehhi A, Kingsley K (2014) Water saturation uncertainty of tight, microporosity dominated carbonate reservoirs and the impact of hydrocarbon volume; case study from Abu Dhabi, UAE. In: Paper presented at the SPWLA 55th Annual Logging Symposium held in Abu Dhabi, UAE, May 18–22
- Folk RL (1959) Practical petrographic classification of limestones. AAPG Bull 43:1–38
- Griffiths R, Carnegie A, Gyllensten A, Ribeiro MT, Prasadjo A, Sallam Y (2006) Evaluation of low resistivity pay in carbonates—a breakthrough. Society of Petrophysicists and Well-Log Analysts. In: Paper E presented at the SPWLA 47th Annual Logging Symposium held in Veracruz, Mexico, June 4–7
- Gyllensten A, Radwan ES, Al Hammadi MI, Maskary SS (2007) A new saturation model for low resistivity pay in carbonates, SPWLA, PP7
- Hassan A, Kerans C (2013) Rock fabric characterization in a low resistivity pay zone from a Lower Cretaceous carbonate reservoir in the Middle East. In: 2013 SEG Annual Meeting. Society of Exploration Geophysicists
- Keith BD, Pittman ED (1983) Bimodal porosity in oolitic reservoir—effect on productivity and log response, Rodessa limestone (Lower Cretaceous), East Texas basin. AAPG Bull 67(9):1391–1399
- Khan M, Ashqar A, Al Rawahi M, Gashut M (2016) Advances in pulse neutron capture in evaluating formation properties within low permeability carbonates reservoir onshore Abu Dhabi: an integrated case study, SPE 182985-MS
- Obeidi A, Al Aryani F, Al Amoudi M (2010) Developed approach for better understanding of low resistivity pay carbonate reservoirs. In: Paper SPE-137663 presented at Abu Dhabi International Conference and Exhibition, Abu Dhabi
- Petricola MJ, Takezaki H, Asakura S (2002) Saturation evaluation in Micritic Reservoirs: raising to the challenge. In: Abu Dhabi International Petroleum Exhibition and Conference. SPE 78533 Society of Petroleum Engineers
- Pittman ED (1971) Microporosity in carbonate rocks. AAPG Bull 55(10):1873–1881
- Rebelle M, Al Nuaimi MA (2006) Lithofacies, depositional environment, and high-resolution sequence Stratigraphy interpretation of reservoir-X, Field A. ADCO Internal Report
- Salahuddin AA, Gibrata MA, Uchida M, Al Hammadi KE, Binmadhi AK (2015) Innovative integration of subsurface data and history matching validation to characterize and model complex carbonate reservoir with high permeability streaks and low resistivity pay issues, onshore Abu Dhabi. In: SPE Reservoir Characterisation and Simulation Conference and Exhibition. SPE-175682
- Scholle PA (2002) A color illustrate guide to carbonate rock constituents, textures, cements, and porosities. AAPG Memoir 27
- Scholle PA, Ulmer-Scholle DS (2003) A color guide to the petrography of carbonate rocks: grains, textures, porosity, diagenesis. AAPG Memoir 77 (Vol. 77). AAPG
- Souvick S (2003) Low-resistivity pay (LRP): ideas for solution. In: Paper SPE-85675 presented at Nigeria Annual International Conference and Exhibition. Society of Petroleum Engineers
- Strohmeinger CJ, Weber LJ, Ghani A, Rebelle M, Al-Mehsin K, Al-Jeelani O, Suwaina O (2004) High-resolution sequence stratigraphy of the Kharab Formation (Lower Cretaceous, UAE). In: Paper SPE-88729 presented at Abu Dhabi International Conference and Exhibition. Abu Dhabi
- Strohmeinger CJ, Weber LJ, Ghani A, Al-Mehsin K, Al-Jeelani O, Al-Mansoori A, Al-Dayyani T, Vaughan L, Khan SA, Mitchell JC (2006) High-resolution sequence stratigraphy and reservoir characterization of Upper Thamama (Lower Cretaceous) reservoirs of a Giant Abu Dhabi Oil Field, United Arab Emirates. AAPG Memoir 88/SEPM Special Publication, p. 139–171
- Talabani S, Boyd D, El Wazeer F, Al Arfi S (2000) Validity of Archie equation in carbonate rocks, SPE 87302
- Uchida M, Salahuddin AA, Ashqar A, Awolayo AN, Olayiwola SO, Al-Hammadi EK (2015) Evaluation of water saturation in a low-resistivity pay carbonate reservoir onshore Abu Dhabi: an integrated approach. In: Paper SPE 177709MS presented at Abu Dhabi International Conference and Exhibition
- Worthington PF (2000) Recognition and evaluation of low-resistivity pay. *Pet Geosci* 6(1):77–92
- Zhao ZZ, Ouyang J, Liu DL (2000) Logging technology and interpretation techniques for low-resistivity pay in Bohai Bay Basin. Petroleum Industry Press, Beijing